Tellus (1995), 47A, 1032–1046
Printed in Belgium – all rights reserved

TELLUS
ISSN 0280–6495

Bifurcation of eastward jets induced by mid-ocean ridges and diverging isobaths

By CHUAN SHI[1]* and SHENN-YU CHAO, *University of Maryland, Center for Environmental and Estuarine Studies, Horn Point Environmental Laboratory, Cambridge, Maryland 21613-0775, USA*

(Manuscript received 29 August 1994; in final form 2 November 1994)

ABSTRACT

A three-dimensional primitive-equation model is employed to investigate how a mid-ocean ridge affects an eastward incoming jet overlying isobaths that diverge eastward. The diverging isobaths contain a major northeastward continental slope and a minor deeper southeastward bottom slope, both with shallow waters to the north. The southwest-northeast trending mid-ocean ridge is placed at about 1700 km east of the northeastward continental slope. In the barotropic regime, the diverging isobaths force an initially eastward jet to widen and follow f/h contours after a hydraulic jump. The mid-ocean ridge radiates barotropic Rossby waves, further enhancing the lateral widening of the jet. The northern portion of the jet expands northward and forms a western boundary current along the northeastward continental slope. The bifurcated current system consists of the northeastward flow and the remnant of the original eastward current. When the ridge is removed, the jet diverges but does not bifurcate. In the baroclinic regime, continuous meander and eddy activities reinforce the meridional spreading of the jet and cause greater portion of the jet to diverge northward. Consequently, a stronger western boundary current is formed along the northeastward continental slope. As in the barotropic regime, the mid-ocean ridge exerts its influence upstream by radiating barotropic Rossby waves westward, further enhancing the jet splitting. Among possible applications, the model is particularly relevant to the bifurcation of the Gulf Stream as it passes by the southern tail of the Grand Banks.

1. Introduction

The Gulf Stream bifurcates as it passes by the southern tail of the Grand Banks (Fig. 1). The northern branch, commonly known as the North Atlantic Current, flows northeastward and eventually reaches western Europe. The remaining Gulf Stream water either continues eastward or southeastward. Sandwiched in between is an anticyclonic gyre in the Newfoundland Basin. The northern branch is likely important to the western European climate; the vast amount of heat that it carries may be partially responsible for the warming of western Europe in winter.

Observations lend strong support to the Gulf Stream branching near the Grand Banks (Mann, 1967; Clarke et al., 1980; Fofonoff and Hendry, 1985; Sy, 1988; Klein and Siedler, 1989; Krauss et al., 1990; Richardson, 1993). However, the physical mechanisms of this critical breakdown region have not been analyzed. This is in stark contrast to the full attention given to the problems of the Gulf Stream separation from the coast near Cape Hatteras and its interaction with the South Atlantic Bight and the New England Seamount Chain by the modeling community (e.g., Oey et al., 1992; Ezer and Mellor, 1992; Ezer, 1994). As a result, we have little to go by in predicting the degree of the Gulf Stream branching and the consequent volume transport of the North

[1] Now at NASA/Goddard Space Flight Center, Laboratory for Hydrospheric Processes, Mail Code 971, Greenbelt, MD 20771, USA. E-mail: chuan@maya.gsfc.nasa.gov.
* Corresponding author.

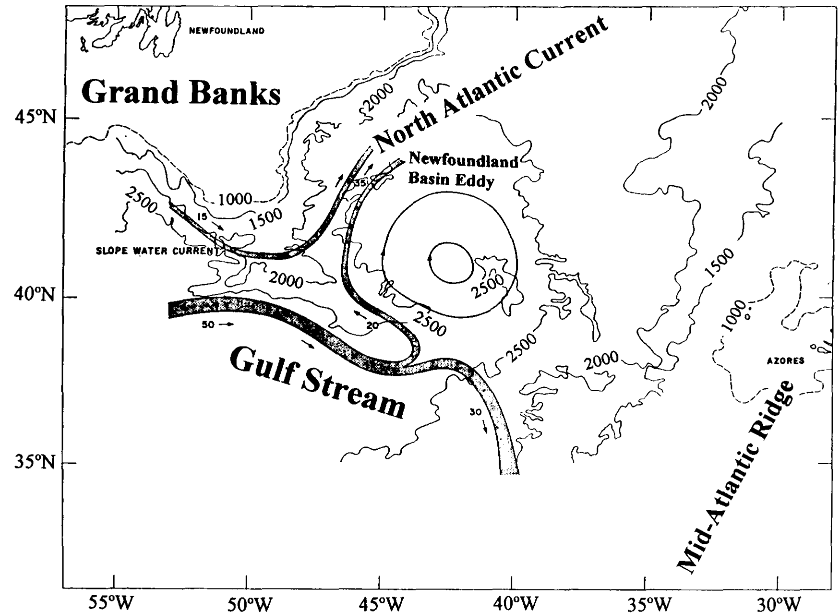

Fig. 1. The current system southeast of the Grand Banks (Mann, 1967), showing the bifurcation of the Gulf Stream. Selected isobaths are labeled in fathoms with intervals of 500 fm.

Atlantic Current. Warren (1969) employed a linear, inviscid, steady, analytical model to demonstrate an eastward jet splitting as it flows over diverging isobaths on an f plane. The barotropic jet bifurcates and follows the diverging isobaths according to conservation of potential vorticity. His linear model assumed that disturbances inside the jet traveled only from upstream to downstream. As a result, branching occurs only for flows with a small Rossby number and generally diminishes with increasing incoming jet speed.

Shi and Chao (1994) (hereafter as SC) examined the response of an initially eastward jet to an eastward diverging isobaths using a three-dimensional primitive-equation numerical model with a free surface on a β plane. The numerical model with seven vertical layers was essentially based on the Princeton Ocean Model (Mellor, 1993) but without the turbulent scheme. The model bottom topography is similar to Warren's (1969), except the gradients and orientations of eastward-branching isobaths are finely turned to retain essential features of bathymetries near the Grand Banks. In the barotropic regime, the model shows that the jet widens but does not bifurcate downstream. The widening is achieved by a hydraulic jump. In the baroclinic regime, the topographic influence is still present but somewhat weakened by stratification. The hydraulic jump process was reinforced by the dissipation due to continuous meander and eddy activities. In contrast to the barotropic jet, the baroclinic jet bifurcates and generates a northeastward branch along the northeastward continental slope. The transport of the northeastward flow is about 20% of the total incoming transport, far below observation-based estimates.

Recent numerical investigation (Chao, 1994) showed that a ridge exerts its influence far upstream by widening the jet if the zonal jet profile is deep enough to "'feel" the ridge. This conclusion holds regardless of whether the deep abyssal current is eastward or westward. The upstream widening of the jet is achieved through westward propagation of barotropic Rossby waves induced by the ridge. Because the jet divergence is a precursor of bifurcation, the addition of a downstream ridge to the previous model of SC may enhance the northeastward branch and bring the model closer to reality. This was the underlying reason motivating the present study.

This work continues the effort of SC by adding a bottom ridge to the east of bifurcated isobaths. To examine how the current system responses to topographic forcing, we are left with two alternatives. One is to specify inflows and outflows at climatological positions (Ezer and Mellor, 1992). This method falls back on empiricism but pushes the model closer to reality. The second alternative is to fix the inflow and outflow at their initial positions regardless of flow adjustment in the model interior (e.g., SC). The latter approach is adopted here because it does not rely on empiricism and allows us to better identify the physical processes. This is achieved at the expense of computational costs because open boundaries must be moved

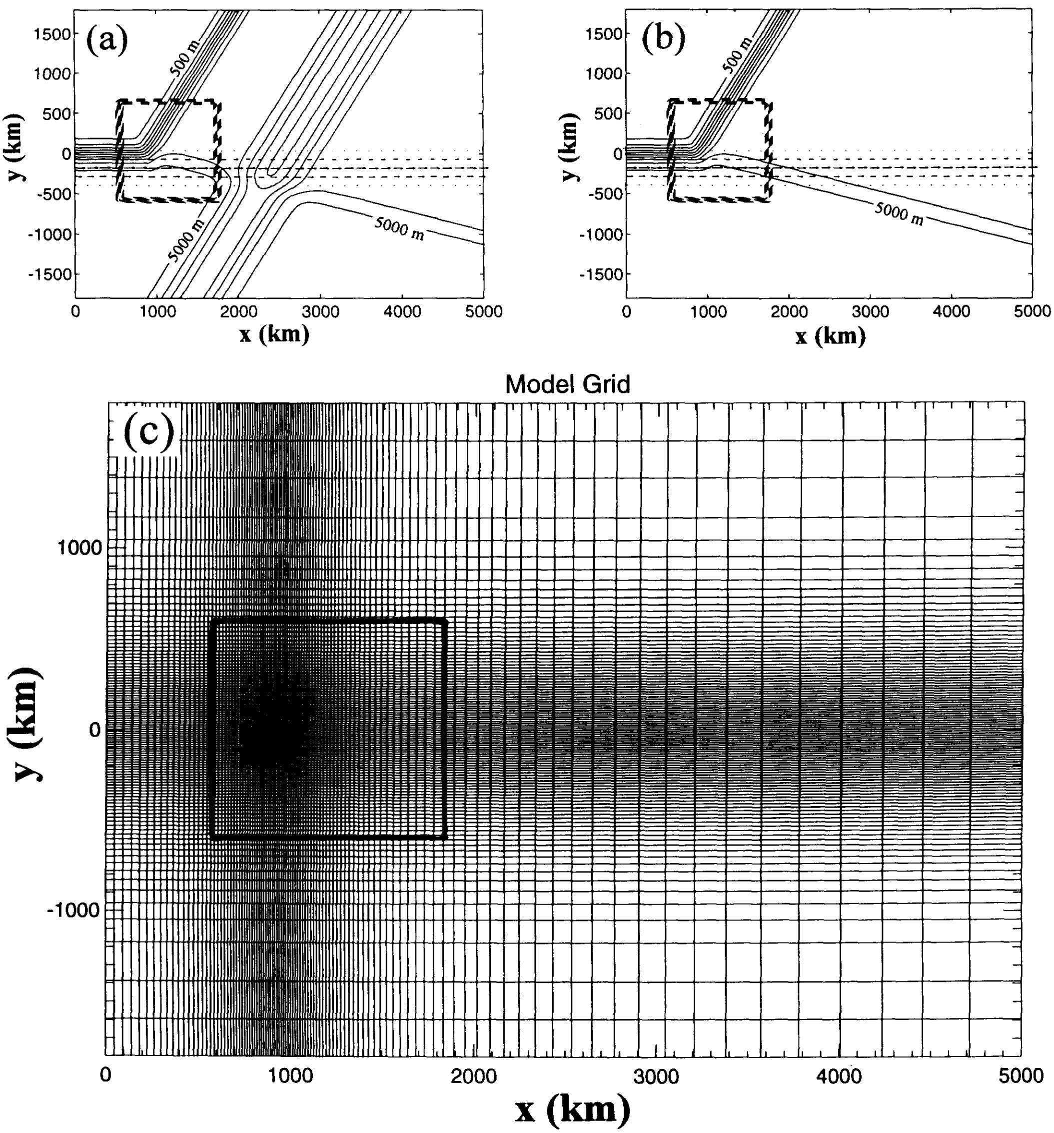

Fig. 2. (a) Initial jets over model bottom topography with a mid-ocean ridge east of bifurcated isobaths, (b) without the ridge, and (c) model grid. Square inserts show the domain of interest. The location and height of the ridge is subject to alteration later. Selected isobaths are labeled in meters with intervals of 500 m.

sufficiently away to lessen their grips on interior solutions.

The adjustment problem is formulated as follows. Initially, an eastward and zonally uniform current with a constant mass transport is specified near the center latitude of the model domain (Figs. 2a, b). The meridional bottom slope under the jet in the west is much steeper than that in the east. In the western portion of the basin, the diverging isobaths contain a major northeastward continental slope (across which the water depth increases from 200 m to 4500 m) and a deeper minor southeastward tending bottom slope (across which the water depth varies from 4500 m to 5200 m). A southwest-northeast trending mid-ocean ridge is placed approximately 1700 km east of the longitude where isobaths begin to diverge. The ridge is chosen to parallel the northeastward isobaths to its west. Subsequent evolution of the eastward jet is dominated by topographic forcing. The model bottom topography (Fig. 2a) is chosen to mimic the realistic smoothed topography of the North Atlantic region from the Grand Banks to the Mid-Atlantic Ridge (Fig. 1). Analytical expression of topography allows for easy alteration of bottom relieves, a needed exercise in order to isolate the role of each topographic forcing. Most importantly, flow adjustment with the ridge will be compared to that without the ridge (Fig. 2b). The computation domain as shown in Fig. 2 is about 12 times larger than the domain of interest. This measure allows interior solutions to evolve mostly free from imperfect open boundary conditions far upstream and downstream.

In the context of geophysical fluid dynamics, the subject of upstream influence exerted by bottom topography does not lend itself to simple analytical treatment. Even in the nonrotating limit, the possible upstream influence for stratified flows over obstacles remains unresolved for 40 years after Long (1955) established the steady state model. Serious efforts to resolve it often lead to raging controversies, still unresolved (Yih, 1980). Systematic investigation of upstream influences for eastward jets over obstacles on a β plane lags far behind its nonrotating counterpart. Lacking analytical solution recourse limits the present approach to be strictly numerical.

The paper is organized as follows. Section 2 describes the numerical model. In Section 3, the adjustment processes of eastward jets are studied using the barotropic version of the present model. In Section 4, the subject is reinvestigated in the baroclinic regime. A general discussion and possible applications to the current system near the Grand Banks are given in Section 5.

2. Model description

The model essentially follows the Princeton Ocean Model (Mellor, 1993) but without the turbulent scheme. It employs a σ-coordinate with seven vertical layers and a stretched Cartesian coordinate system in the horizontal directions. The model has a free surface and resolves barotropic and baroclinic components with different time steps. The external mode utilizing a short time step solves for three variables: the vertically average velocity (U, V) and sea surface elevation (η). The internal mode using a long time step solves for four variables: the three-dimensional velocity (u, v, ω) and the temperature (T). Salinity is assumed to be constant. For simplicity, frictional coefficients are assumed to be constant in time. To achieve approximately uniform damping rate for grid-scale noises in a variable grid system, coefficients of horizontal viscosity (A_{m}) and horizontal diffusivity (A_{h}) are grid-dependent. Coefficients of vertical viscosity (K_{m}) and vertical diffusivity (K_{h}) are grid-independent and constant.

The model is configured in a $5000\ \mathrm{km} \times 3600\ \mathrm{km} \times 5.2\ \mathrm{km}$ rectangular box with a coordinate system (x, y, σ), where x and y are eastward and northward, respectively; and σ is upward. The water depth $[h(x, y)]$ is specified by:

$$\begin{aligned} h(x, y) &= h_0 - H_{\mathrm{rdg}} \exp\{-[(x - y/s_1 - X_{\mathrm{rdg}})/L_{\mathrm{rdg}}]^2\} \\ &\quad -(\Delta h_1 + \Delta h_2)\tanh(\alpha_0 y) \\ &\quad \text{for} \quad x < x_0 - y(\gamma - 1)/s_1, \\ h(x, y) &= h_0 - H_{\mathrm{rdg}} \exp\{-[(x - y/s_1 - X_{\mathrm{rdg}})/L_{\mathrm{rdg}}]^2\} \\ &\quad -\Delta h_1 \tanh\{\alpha_0[y - s_1(x - x_0)]/\gamma\} \\ &\quad -\Delta h_2 \tanh\{\alpha_0[y - s_2(x - x_0 + y(\gamma - 1)/s_1)]\} \\ &\quad \text{for} \quad x \geqslant x_0 - y(\gamma - 1)/s_1. \end{aligned}$$

The origin of the coordinate system $(x = 0, y = 0)$ is placed at the middle point of the western boundary. Typical values of bottom topographic parameters are: $h_0 = 2700\ \mathrm{m}$, $\Delta h_1 = 2100\ \mathrm{m}$, $\Delta h_2 = 400\ \mathrm{m}$, $H_{\mathrm{rdg}} = 2\ \mathrm{km}$, $X_{\mathrm{rdg}} = 2600\ \mathrm{km}$, $L_{\mathrm{rdg}} =$

360 km, $\alpha_0 = 1/130\ (\mathrm{km})^{-1}$, $x_0 = 900$ km, $s_1 = 1.6$, $s_2 = -0.3$, and $\gamma = (1 + s_1^2)^{1/2} = 1.9$. Isobaths with and without the ridge are shown in Figs. 2a, b. Stretched coordinates $\{X = \tanh[3.3(x - x_0)/\lambda]$ and $Y = \tanh(2y/\lambda)\}$ are introduced with $\lambda = 1200$ km, so that $0 \leqslant X \leqslant 1$ (for $0 \leqslant x < \infty$), and $-1 \leqslant Y \leqslant 1$ (for $-\infty < y < \infty$). The variables Δx and Δy can be determined from: $\Delta x = \lambda \cosh^2(x/\lambda)\, \Delta X$ and $\Delta y = \lambda \cosh^2[2(y/\lambda)]\, \Delta Y/2$ (Fig. 2c). With $\Delta X = 1/101$ and 100 meshes in the zonal direction, Δx varies from 12 km at $x = x_0 = 900$ km (i.e., at the westernmost point of bifurcated isobaths) to 46 km at the western boundary ($x = 0$) and 280 km at the eastern boundary ($x = 5000$ km) (Fig. 2c). Similarly, with $\Delta Y = 2/101$ and 100 meshes in the meridional direction, Δy varies from 12 km at the central latitude ($y = 0$) to 215 km at the northern and southern boundaries ($y = \pm 1800$ km) (Fig. 2c). Between the free surface ($z = \eta$) and the bottom [$z = -h(x, y)$], the topography-following σ coordinate is determined by $\sigma = (z - \eta)/[h(x, y) + \eta]$. Therefore, σ ranges from 0 at $z = \eta$ to -1 at $z = -h(x, y)$.

2.1. *Initial conditions*

For the barotropic study, the eastward geostrophic jet is initially Gaussian:

$$V_{\mathrm{in}} = 0, \tag{1a}$$

$$U_{\mathrm{in}}(y) = U_0 \exp\left[-\left(\frac{y - Y_0}{L}\right)^2\right] h_n/h(x, y), \tag{1b}$$

$$\eta_{\mathrm{in}}(y) = -0.5\pi^{1/2} f_0 U_0 L \operatorname{erf}\left(\frac{y - Y_0}{L}\right) \Big/ g, \tag{1c}$$

where L is the initial half-width of the jet, h_{n} is a characteristic basin depth scale, $y = Y_0$ is the initial jet axis, g is the gravitational constant, U_0 is the initial axial speed of the jet, erf( ) is the error function, and the subscript in refers to initial values. The Coriolis parameter is given by $f = f_0 + \beta y$. The initial sea level and current are in geostrophic balance.

For the baroclinic study, the initial eastward jet profile is given by,

$$v_{\mathrm{in}} = V_{\mathrm{in}} = 0, \tag{2a}$$

$$u_{\mathrm{in}} = \frac{2g\, D\alpha\, \Delta T}{\pi^{1/2} f_0 L} \exp\left[-\left(\frac{y - Y_0}{L}\right)^2\right] \times \left[\tanh\left(\frac{z}{D}\right) + \tanh\left(\frac{h_{\mathrm{n}}}{D}\right)\right], \tag{2b}$$

$$T_{\mathrm{in}} = T_0 - \frac{\Delta T}{\cosh^2(z/D)}\left[\operatorname{erf}\left(\frac{y - Y_0}{L}\right) - 1\right], \tag{2c}$$

$$U_{\mathrm{in}} = \frac{2g\, D\alpha\, \Delta T}{\pi^{1/2} f_0 L} \exp\left[-\left(\frac{y - Y_0}{L}\right)^2\right] \times \left\{\tanh\left(\frac{h_{\mathrm{n}}}{D}\right) - \frac{D}{h_{\mathrm{n}}} \ln\left[\cosh\left(\frac{h_{\mathrm{n}}}{D}\right)\right]\right\} \tag{2d}$$

$$\eta_{\mathrm{in}} = -\alpha\, \Delta T D \tanh\left(\frac{h_{\mathrm{n}}}{D}\right) \operatorname{erf}\left(\frac{y - Y_0}{L}\right), \tag{2e}$$

where α is the thermal expansion coefficient relating the water density (ρ) to the temperature (T) by $\rho = \rho_0(1 - \alpha T)$, $2\,\Delta T$ is the initial sea surface temperature variation across the jet, and D is the characteristic depth scale of the jet. The sea surface temperature varies from T_0 north of the jet to $T_0 + 2\,\Delta T$ south of it. From north to south, the sea surface elevation (η) changes from $-\alpha\, \Delta T D \tanh(h_{\mathrm{n}}/D)$ to $\alpha\, \Delta T D \tanh(h_{\mathrm{n}}/D)$. The initial temperature field (T_{in}) is in geostrophic balance with the initial zonal velocity (u_{in}), assuming $z = -h_{\mathrm{n}}$ is the level of no motion.

Unless otherwise stated, typical values of parameters used in this study are: $g = 9.8$ m/s^2, $\rho_0 = 10^3$ kg/m^3, $D = 1000$ m, $h_{\mathrm{n}} = 4000$ m, $f_0 = 10^{-4}\ \mathrm{s}^{-1}$, $\beta = 2 \times 10^{-11}\ \mathrm{s}^{-1}\ \mathrm{m}^{-1}$, $U_0 = 0.4\ \mathrm{m\ s}^{-1}$, $L = 40$ km, $Y_0 = -(2\alpha_0)^{-1} = -65$ km, $T_0 = 6$°C, $\Delta T = 8$°C, $\alpha = 10^{-4}\,(°\mathrm{C})^{-1}$, $A_{\mathrm{m}} = 20 A_{\mathrm{h}} = (0.8 \times 10^{-5})\, \Delta x^2\, \Delta y^2/(\Delta x^2 + \Delta y^2)$ (m^2 s^{-1}), and $K_{\mathrm{m}} = 10 K_{\mathrm{h}} = 10^{-4}\ \mathrm{m}^2\,\mathrm{s}^{-1}$. With the choice of $D = 1000$ m, the baroclinic jet is essentially confined to above 1000 m depth and attenuates rapidly further downward.

2.2. *Boundary conditions*

There are no mechanical or thermal forcing at the sea surface and a quadratic stress is placed at the bottom with a dimensionless drag coefficient of 0.0025. Horizontal boundary conditions follow essentially those of SC and are briefly described below. There are seven variables (η, T, u, U, v, V, ω) to be constrained along the horizontal boundaries. The horizontal boundary condition for the sea surface elevation (η) is one of no normal gradient across all the boundaries. For the vertical velocity, $\omega = 0$ on all boundaries. Along the southern and northern boundaries, the conditions for the zonal and meridional velocity (u, v, U, V) and temperature (T) are free-slip for u and

U, $v = V = 0$, and $T = T_{in}$. The western and eastern boundaries are open for inflow and outflow, respectively. Save for transport fluctuations associated with barotropic gravity waves, $U = U_{in}$ and $V = 0$ on both western and eastern boundaries (Mellor, 1993). On these two boundaries, the current deviations from vertical means, $(u', v') = (u - U, v - V)$, are extrapolated from nearest interior grid points.

3. Barotropic results

A dimensionless parameter dictating the jet behavior in the barotropic regime is the Froude/Rossby number, defined as

$$R_\beta = \frac{U}{(\beta + \beta_h)\, L^2},$$

where $\beta_h = -f/h\, \partial h/\partial y$ is the topography vorticity gradient. The number measures the strength of the eastward jet against $(\beta + \beta_h)$-induced Rossby waves propagating westward, similar to the Froude number of the open channel flow. In the latter case, however, the upstream propagation is achieved by gravity waves, internal and external alike. In the absence of β_h, Armi (1989) established that the critical Froude/Rossby number is approximately 0.25; the jet is supercritical above it and subcritical below it. SC showed that the addition of a bottom slope does not change this approximate criterion. Table 1 lists parameters and crucial results from barotropic experiments. It should be emphasized that the initial jet is supercritical everywhere. The initial Froude/Rossby number is 0.61 upstream (at $x = 600$ km) and increases to 7.1 downstream (at $x = 1800$ km) due to the eastward decrease in meridional bottom slope.

3.1. Control runs

Fig. 3 shows the vertically averaged flow fields inside the domain of interest at day 80 for cases without and with the ridge as final states of flow fields. As was shown in Table 1, the incoming transport entering the basin is 100 Sv. With the mid-ocean ridge (Fig. 3), the jet bifurcates with a northern branch transporting 29 Sv of water northeastward; the remaining 71 Sv continues eastward or southeastward. The transport of the northern branch (ψ_n) is measured here and after as that exiting the northern boundary of the domain of interest (i.e., $y = 600$ km and $600 \text{ km} \leqslant x \leqslant 1800$ km). Without the mid-ocean ridge (Fig. 3 top), the jet diverges downstream but does not bifurcate (i.e., $\psi_n = 0$).

In the absence of the ridge, the incoming jet over the steep meridional bottom slope turns cyclonically as it enters deeper waters near $x = 1100$ km,

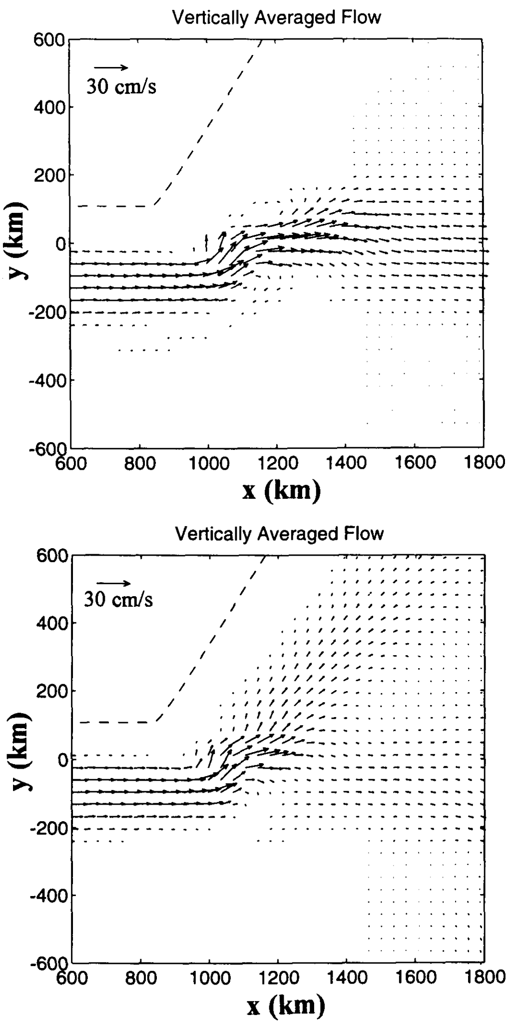

Fig. 3. Vertically averaged flow fields for the cases without the ridge (top) and with the ridge (bottom) from the barotropic model at day 80. The eastward jet diverges without the ridge but bifurcates with the ridge. Dashed lines indicate the 1000 m isobath.

Table 1. *List of barotropic experiments, northward transports (ψ_N) and upstream Froude/Rossby numbers at day 80*

Total incoming transport (ψ_W) $\approx$ 100 Sv, initial R_β ($x = 600$ km) = 0.61

Cases #	H_{rdg} (km)	L_{rdg} (km)	X_{rdg} (km)	ψ_N (Sv)	R_β ($x = 600$ km)
(a) (control run)	2	360	2600	29	0.17
(b)	1	360	2600	13	0.16
(c)	1	180	2600	20	0.18
(d)	1	180	3400	17	0.17
(e) (no ridge)	0	—	—	0	0.24

becoming essentially an inertial western boundary current following the northeastward isobaths. The behavior is in keeping with the potential vorticity conservation. The northeastward current gains planetary vorticity and consequently suffers a like amount of loss in relatively vorticity, forcing the jet to turn anticyclonically and flow eastward again. The eastward jet then undergoes a sudden expansion near $x = 1400$ km because of a hydraulic jump. Detailed vorticity and momentum analyses relating to the jet path and hydraulic jump were presented earlier in SC and therefore will not be repeated here.

To quantify further, the resulting Froude/Rossby number at day 80 is nearly critical upstream (i.e., $R_\beta = 0.24$ at $x = 600$ km). The jet becomes supercritical ($R_\beta = 1.6$ at day 80) at where it turns northeastward ($x = 1100$ km) as a consequence of western intensification. Far downstream ($x = 1800$ km), the jet becomes subcritical ($R_\beta = 0.1$ at day 80) after the hydraulic jump. As in the case of open channel hydraulics, the hydraulic jump is maintained by an upstream control and a downstream control. The former is caused by the northeastward isobaths east of the banks that narrow the jet through the mechanism of western intensification, maintaining the jet to be supercritical. The latter is due to diverging isobaths that induce the jet to follow diverging f/h contours and become subcritical. The model dependence on incoming jet speeds, $\beta + \beta_h$, and other pertinent parameters was explored earlier in SC and will not be repeated here.

In addition to diverging isobaths, the mid-ocean ridge provides a second means of the downstream control. The jet over diverging isobaths becomes even more subcritical caused by the westward radiation of ridge-induced Rossby waves. Barotropic Kelvin waves should be ruled out, having phase speeds on the order of 10000 km/day, about 50 times greater than the dominant phase speeds to be discussed below. As a result, the enhanced jet divergence west of the ridge eventually leads to visible bifurcation, with a stationary northern branch manifested as a western boundary current along the eastern flank of the banks (Fig. 3 bottom). The visible branching entails a loss of definition of R_β downstream. Over the zonal isobaths upstream, R_β decreases slightly due to the presence of the downstream ridge (see Table 1). Apparently, the upstream influence exerted by the ridge penetrates west of the longitude where isobaths begin to diverge.

Since barotropic Rossby waves are primarily responsible for the upstream influences, their characteristics can best be illustrated by longitude-time ($x - t$) plots of vertically averaged meridional currents. Fig. 4 show such slices taken along the center latitude ($y = 0$) for the cases with and without the ridge. In both cases, westward propagation of Rossby waves as indicated by the negative slopes of the contours is evident between $x = 1200$ km and $x = 2000$ km, but their phase speeds, periods and frequency of occurrence differ. These waves are generally aperiodic, dispersive, and dampened in time. In the first seven days, there are three groups of waves propagating westward between $x = 1200$ km and $x = 2000$ km in the case with the ridge, but there is only one without the ridge. This result alone evidences the upstream influence exerted by the ridge. After about 10 days, Rossby wave coming from far downstream decelerates continuously along its track westward, and are eventually arrested near $x = 1400$ km where the jet begins to either diverge or bifurcate. West of $x = 1200$ km, a stationary

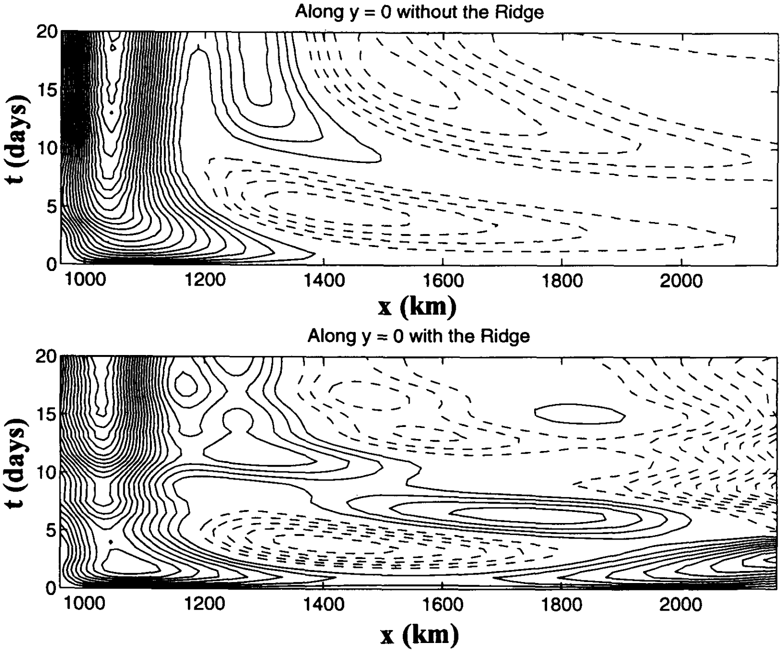

Fig. 4. Longitude-time sections of vertically averaged meridional current at $y = 0$ without the ridge (top) and with the ridge (bottom). The two panels correspond to the top and bottom panels of Fig. 3, respectively. The contour interval is 0.5 cm/s. Solid and dashed contours correspond to positive and negative values, respectively.

northward current intensifies continuously whether the ridge is present or not. It should be emphasized that these waves owe their existence to divergent isobaths and the mid-ocean ridge; their intensity diminishes in time as both current systems are approaching steady states after 20 days.

In the first 10 days, the dominant westward phase speed between $x = 1200$ km and 1800 km is about 180 km/day with the ridge and about 100 km/day without the ridge. The dominant period is about 7 days with the ridge and about 8 days without the ridge. The corresponding zonal wavelength is about 1260 km for the ridge case and about 800 km for the no-ridge case. The former is compatible with the zonal distance between the ridge and the eastern flank of the banks (about 1700 km). With $\beta = 2 \times 10^{-11}\ \mathrm{m^{-1}\ s^{-1}}$ and $\beta_h = 1.5 \times 10^{-11}\ \mathrm{m^{-1}\ s^{-1}}$ near $x = 1800$ km, the approximate dispersion relation, $C_x = -(\beta + \beta_h)/(4\pi^2/L_x^2 + 4\pi^2/L_y^2)$, leads to a meridional wavelength ($L_y = 2773$ km) with the ridge and an imaginary meridional wavelength ($L_y = i\,1116$ km) without the ridge. The simple estimate suggests that the Rossby waves are meridionally extensive in the presence of the ridge, but are mainly concentrated along the jet axis and attenuate meridionally without the ridge.

Figs. 5, 6 show temporal evolution of streamlines in the domain of interest from day 5 to day 13 with and without the ridge. Without the ridge (Fig. 5), the jet diverges but does not bifurcate downstream. The northernmost streamline, once separated from the mainstream, shows modest meridional oscillation at first but becomes increasingly stationary in time. Western propagation of Rossby waves is evident south of the jet. Rossby wave activities are not meridionally expansive. In contrast, the case with the ridge (Fig. 6) reaffirms the earlier analysis that Rossby waves remain active meridionally away from the jet. Western propagation of Rossby waves is evident both north and south of the jet from day 5 to day 9. Thereafter, the northern portion of the jet becomes increasingly stationary and separated

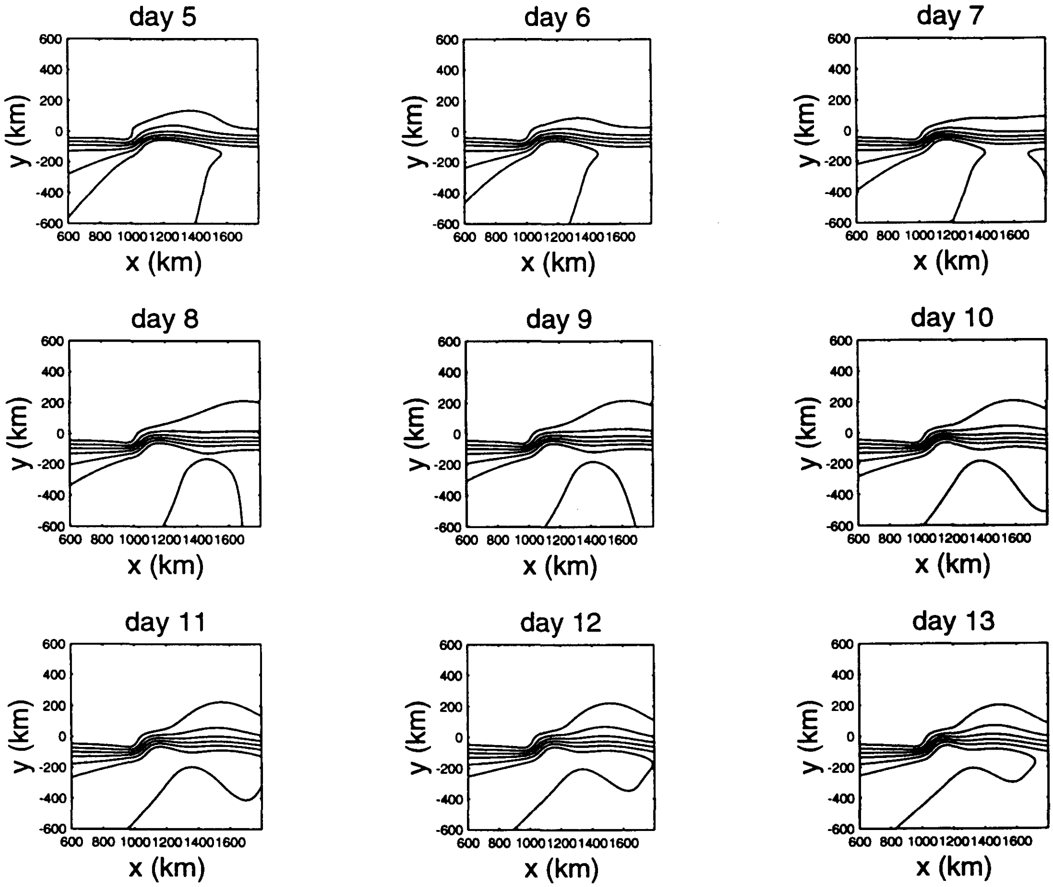

Fig. 5. Temporal evolution of streamlines from day 5 to day 13 at one-day intervals from the barotropic model for the case without the ridge. The northernmost and southernmost contours correspond to the 100 Sv and 0 Sv, respectively; the contour interval is 20 Sv.

from the main jet. Visually, one gets the distinct impression that the jet bifurcation originates from the downstream ridge.

3.2. The rôle of the ridge

Model sensitivity to the ridge height (H_{rdg}) and zonal location of the ridge (X_{rdg}) further confirms the earlier conclusion that the ridge is responsible for the jet bifurcation. When the ridge height decreases from 2 km to 1 km (cases (a) versus (b) in Table 1), the transport of the northern branch is reduced from 29 Sv to 13 Sv. If the ridge is displaced 800 km eastward, the transport of the northern branch decreases slightly from 20 Sv to 17 Sv (cases (c) versus (d) in Table 1). A less intuitive conclusion emerges by comparing case (b) with case (c). As the *e*-folding half-width of the ridge increases from 180 km to 360 km, the transport of the northern branch decreases from 20 Sv to 13 Sv. Note that a narrow ridge (case (c)) exerts only remote influence to the jet path in the domain of interest via westward propagation of Rossby waves. As the width of the ridge expands further westward into the domain of interest (case (b)), the influence of the ridge is no longer remote. The tendency for the jet to follow f/h contours over the westernmost flank of the ridge diverts more transport southward with a wide ridge than with a narrow ridge, reducing the transport available for the northern branch.

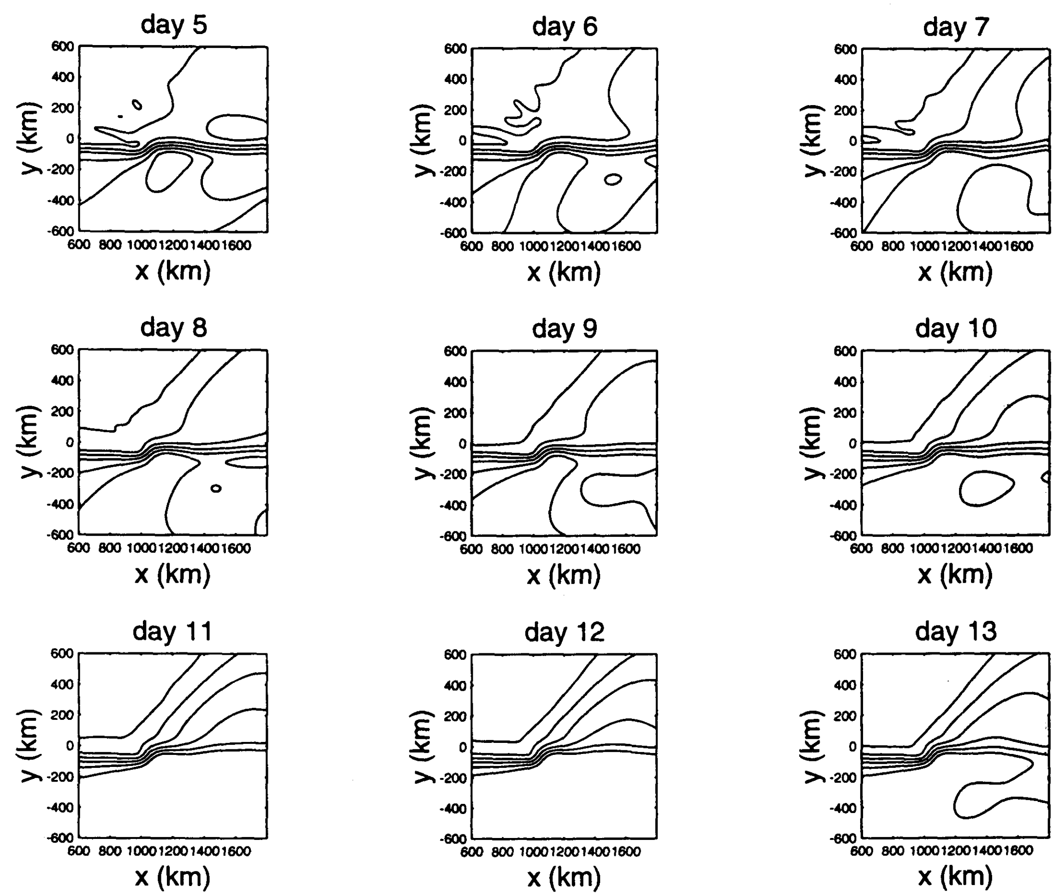

Fig. 6. As in Fig. 5 except with the ridge.

4. Baroclinic results

The baroclinic experiments parallel those in the barotropic regime in which the vertically averaged jets are identical for both cases. The initial R_β in the baroclinic regime is therefore identical to its equivalent in the barotropic regime. Table 2 lists parameters and crucial results for all baroclinic cases.

4.1. Control runs

Fig. 7 shows vertically averaged flow fields with and without the mid-ocean ridge (cases (i) and (v) in Table 2) at day 240. In both cases, the jet bifurcates as it passes by the southern tail of the banks. Of the total transport of 100 Sv, the northern branch carries 22 Sv without the ridge, and 40 Sv with the ridge. It should be noted that the jet separation is essentially completed in about 120 days. Thereafter, continuous perturbation by meanders and eddies does not alter the strength of the two branches.

Without the ridge, the barotropic jet also bifurcates (Fig. 7 top) even though the barotropic jet does not (Fig. 3 top). The former owes its existence to instabilities of the baroclinic current system (see SC for detailed discussion). As the jet leaves the steep bottom slope upstream and enters deep waters, the topographic β effect is much reduced. Continuous meander and eddy activities lead to irreversible meridional expansion of isotherms and currents. The northern portion of the diverging current system, when reaching the eastern flank of the banks, forms a stationary western boundary

Table 2. *List of baroclinic experiments, northward transports (ψ_N) and upstream Froude/Rossby numbers at day 240*

Total incoming transport (ψ_W) $\approx$ 100 Sv, initial R_β ($x = 600$ km) $= 0.61$

Cases #	H_{rdg} (km)	L_{rdg} (km)	X_{rdg} (km)	ψ_N (Sv)	R_β ($x = 600$ km)
(i) (control run)	2	360	2600	40	0.43
(ii)	1	360	2600	39	0.44
(iii)	1	180	2600	55	0.46
(iv)	1	180	3400	50	0.45
(v) (no ridge)	0	—	—	22	0.54

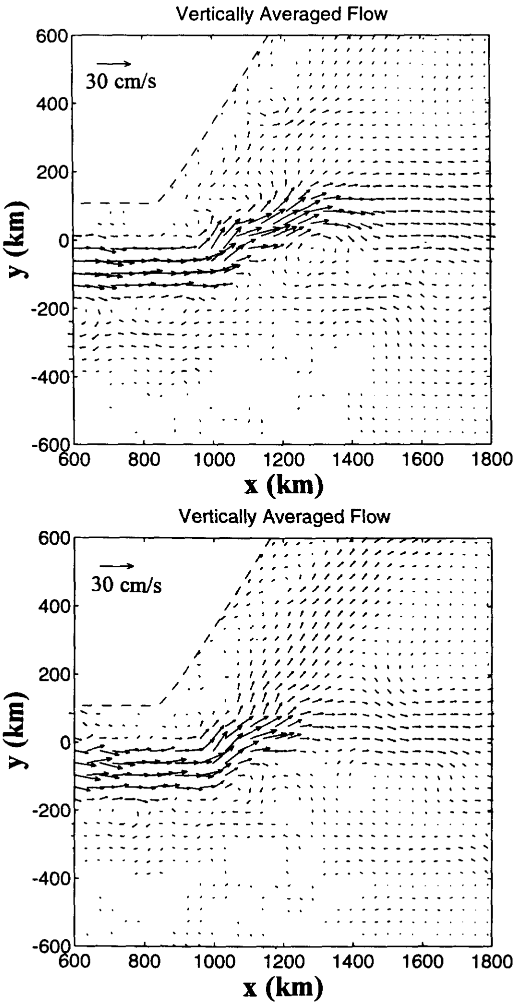

Fig. 7. Vertically averaged flow fields for the cases without the ridge (top) and with the ridge (bottom) from the baroclinic model at day 240. The eastward jet bifurcates in both cases. Dashed lines indicate the 1000 m isobath.

current and separates from the main jet. Over the upstream zonal isobaths, R_β at $x = 600$ km decreases slightly from 0.61 at day 0 to 0.54 at day 80 without the ridge. Thus, stratification shields the upper ocean jet from much of the topography control, which tends to render the jet critical. The downstream jet becomes extremely subcritical if the jet width is measured as that of the two branches combined. As in the barotropic cases, the hydraulic jump still takes place in the baroclinic regime but is reinforced by meander and eddy activities.

The presence of the ridge enhances the transport of the northern branch roughly by a factor of two (Fig. 7, bottom). Farther upstream, the upstream influence exerted by the ridge is much reduced. At $x = 600$ km, R_β is further reduced from 0.54 to 0.43 at day 80 due to the presence of the ridge. Longitude-time slices (not shown) indicate that the westward propagation of barotropic Rossby waves is active only in the case with the ridge, the dominant phase speed being about 170 km/day for the first 20 days or so and decreasing continuously thereafter. Fig. 8 shows currents at 400 m below the sea surface at days 120 and 240 with the ridge. The separation of two branches becomes visually more apparent than the vertically averaged flow fields. Furthermore, the northeastward branch seems stronger and wider than the eastward branch. Because the northeastward branch is in shallower waters, its transport is still less than the transport of the eastward branch. Save for meanders and eddies, these two branches are quite stationary.

With the ridge present, isotherms at 400 m below the sea surface (Fig. 9) fan out sharply as the jet flows over the diverging isobaths, much more so than those without the ridge (not shown). In the downstream region, between $x = 1200$ km and

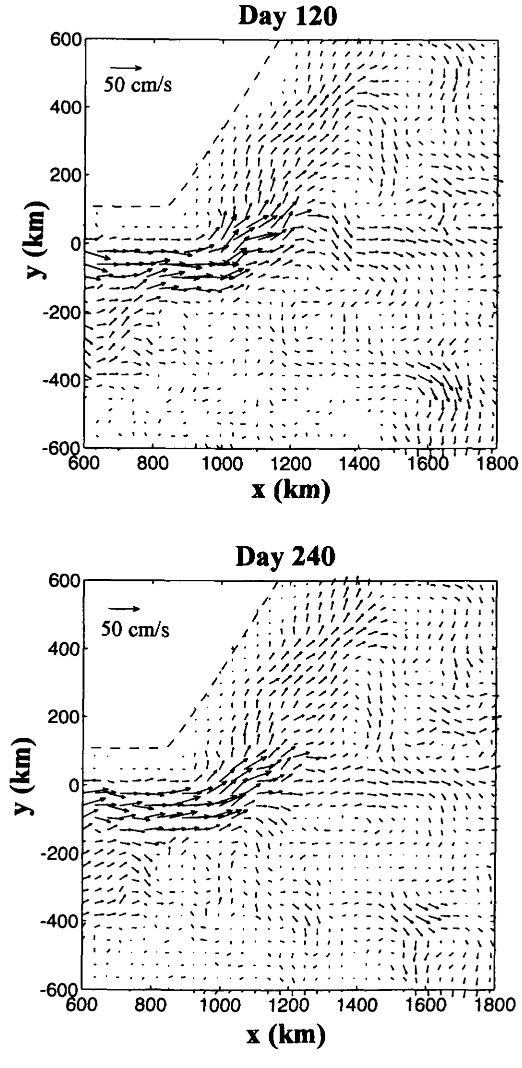

Fig. 8. Currents at 400 m depth with the ridge from the baroclinic model at day 120 (top) and day 240 (bottom). Dashed lines indicate the 1000 m isobaths.

$x = 1800$ km, isotherms tend to be displaced southward. Part of this tendency is caused by meander and eddy activities even without the ridge. Another contribution is the ridge-induced southward velocity component causing the eastward jet to follows f/h contours over the western flank of the ridge, further shifting isotherms southward. From day 120 to day 240, isotherms in the near field ($x < 1200$ km) remain largely stationary; evolution occurs mainly in the far field ($x > 1200$ km).

Figs. 10, 11 show the temporal evolution of vertically integrated streamlines in the domain of interest from day 5 and day 13 with and without the ridge from the baroclinic model. Without the ridge (Fig. 10), the jet divergence proceeds smoothly and becomes increasingly stationary in time. With the ridge (Fig. 11), the jet divergence

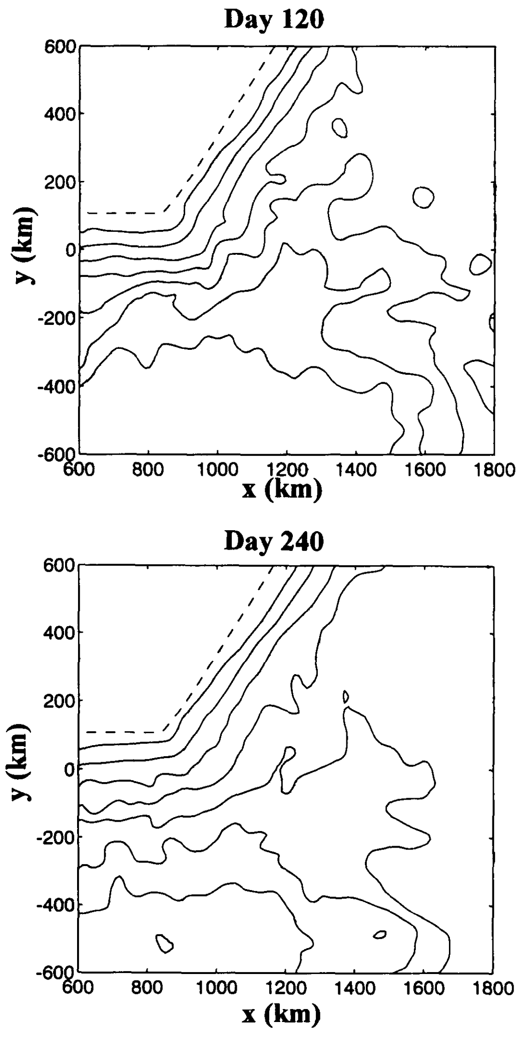

Fig. 9. Isotherms at 400 m depth with the ridge from the baroclinic model at day 120 (top) and day 240 (bottom). Dashed lines indicate the 1000 m isobath. Contour intervals are 2°C, with the northernmost and southernmost isotherms representing 8°C and 20°C, respectively.

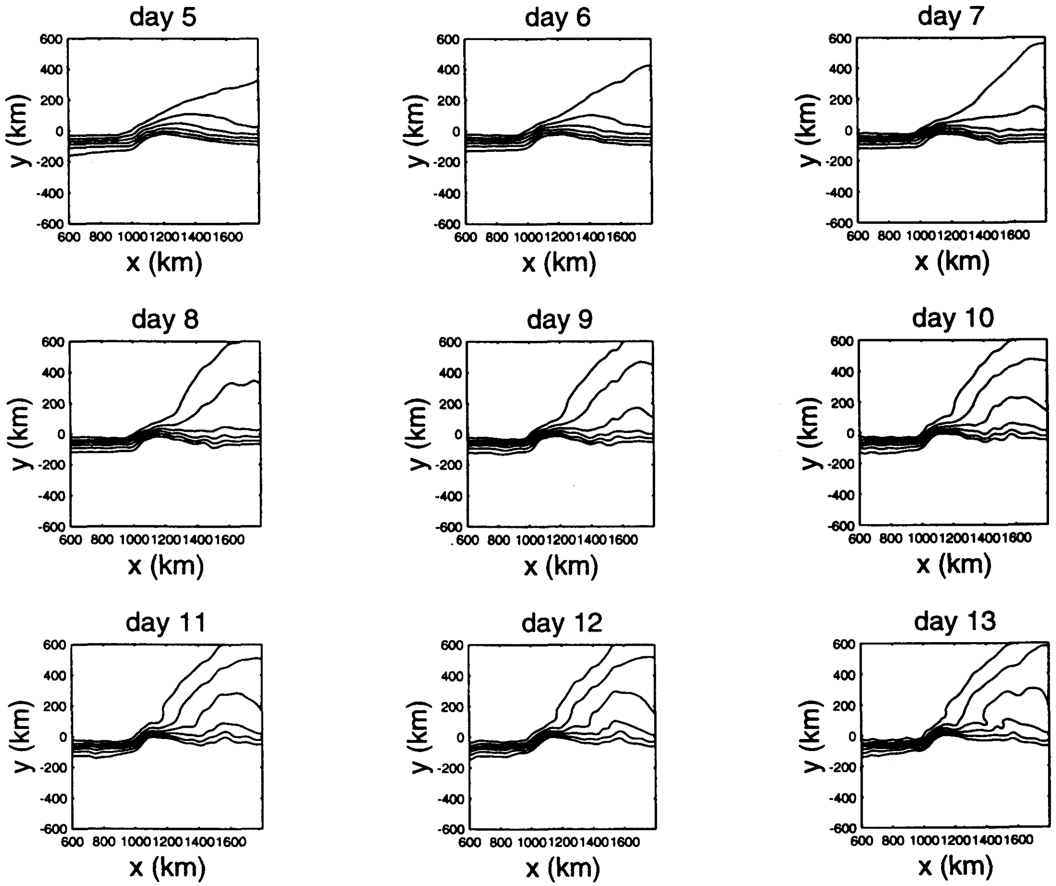

Fig. 10. Temporal evolution of streamlines from day 5 to day 13 at one-day intervals from the baroclinic model without the ridge. The northernmost and southernmost contours correspond to the 100 Sv and 0 Sv, respectively and the contour interval is 20 Sv.

proceeds not as smoothly and the bifurcation occurs slightly earlier. After day 7, the two branches becomes quite visible and increasingly stationary. Visually, the northern branch with the ridge carries a transport almost twice as that without the ridge even in this early stage of development. As in the barotropic regime, oscillations are meridionally more expansive with the ridge than without the ridge. Furthermore, the early expansion of streamlines even in first 10 days again supports the barotropic origin of ridge-enhanced bifurcation.

4.2. *Parameter study*

Model dependence on the ridge as summarized in Table 2 parallels that in the barotropic regime, but the quantitative difference between the two reveals a new feature that warrants discussions. If the ridge height decreases from 2 km (case (i)) to 1 km (case (ii)), the transport of the northern branch decreases only slightly from 40 Sv to 39 Sv. When the height reduces further from 1 km (case (ii)) to 0 km (case (v)), the northward transport decreases by about a factor of two. The model sensitivity to the ridge height appears to exist in a range below 1 km, above which the response of the baroclinic jets becomes saturated. As in the barotropic regime, the transport of the northern branch decreases if the ridge is displaced further eastward (case (iii) versus case (iv)) or if the ridge width increases (case (ii) versus case (iii)). Over the zonal isobaths upstream, R_β at day 240

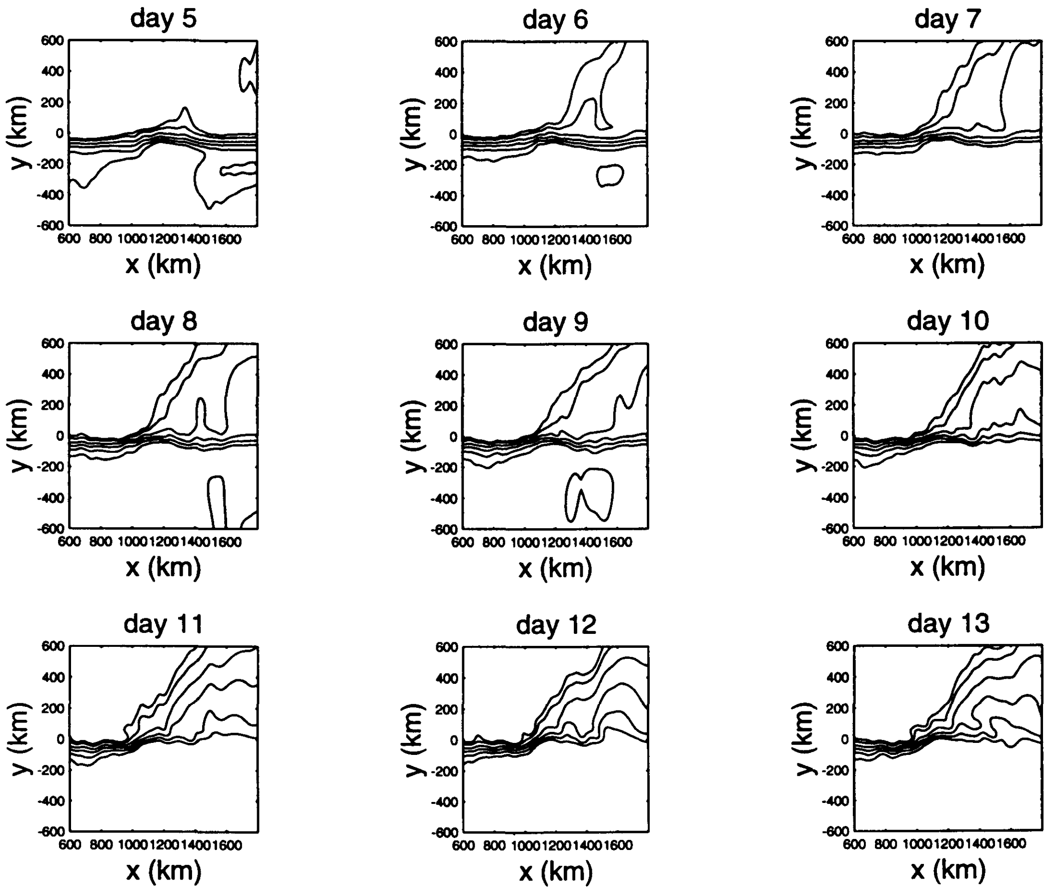

Fig. 11. As in Fig. 10 except with the ridge.

decreases slightly due to the presence of the ridge (Table 2). The strongest northeastward transport is 55 Sv in case (iii).

5. Discussion and conclusions

The westward influence of mid-ocean ridges on incoming jets overlying divergent isobaths is numerically investigated in both barotropic and baroclinic regimes. The model topography is expressed in analytical form to retain essential features of that in the vicinity of the Grand Banks. This choice prohibits quantitative conclusions, but allows for better identification of physical mechanisms at work. The most important conclusion from this work is that the ridge enhances the jet bifurcation upstream of the ridge via westward propagation of barotropic Rossby waves. In the barotropic regime, the jet bifurcation owes its existence to the mid-ocean ridge. In the baroclinic regime, the northern branch is significantly enhanced by the ridge. The transport of the northern branch with the ridge almost doubles that without the ridge. The northern branch intensifies along the eastern flank of the banks as a western boundary current.

The ridge exerts its influence upstream by radiating barotropic Rossby waves. Baroclinic Rossby waves should be ruled out because their phase speeds vanish rapidly with latitudes, unable to penetrate upstream against eastward currents in these high latitudes. The barotropic mechanism ensures a fast adjustment in response to the topographic forcing. In fact, the upstream influence as indicated by the abundance of barotropic Rossby wave propagation is achieved in the early stage of the adjustment. Thereafter, the ridge-induced barotropic Rossby waves are mostly absent as the system approaches steady state. Barotropic Rossby waves originated from downstream are presumably produced by jet-induced unsteady disturbances impinging upon the underlying ridge. In the early stage of adjustment, the phase speeds of these barotropic waves are comparable whether the jet is barotropic or baroclinic.

A more intuitive explanation is that blocking by the ridge simply splits the incoming jet due to conservation of volume. For these disturbances to travel more than 1000 km upstream from the ridge, our analysis suggests that most of them organize as barotropic Rossby waves. We are unable, however, to quantify the relative contributions from wavelike and nonwavelike disturbances.

In the presence of the ridge, the modeled northern branch carries 40% $\sim$ 55% of the incoming transport northeastward in the baroclinic regime. The observation-based estimates are comparable, ranging from 54% (Mann, 1967) to 63% (Clarke et al., 1980). The quantitative aspect of the agreement should not be overemphasized, in view of the facts that the model employs somewhat idealized topography and neglects surface wind and thermohaline forcings. Furthermore, the Newfoundland Basin Eddy (Fig. 1) sandwiched between the two branches is conspicuously missing in the model. Conceivably, the negative mean wind stress curl in the area may be responsible for the generation of the weak anticyclonic eddy. Despite these deficiencies, the model does lead us to conclude that the Mid-Atlantic Ridge plays a crucial rôle in producing the Gulf Stream branching near the Grand Banks.

6. Acknowledgments

During the course of this study, the first author was supported by a postdoctoral fellowship at the University of Maryland Center for Environmental and Estuarine Studies, Horn Point Environmental Laboratory. The University of Maryland Center for Environmental and Estuarine Studies, Contribution 2575.

REFERENCES

Armi, L. 1989. Hydraulic control of zonal currents on a β plane. *J. Fluid Mech.* **201**, 357–377.

Chao, S.-Y. 1994. Zonal jets over topography on a β plane, with applications to the Kuroshio Extension over the Shatsky Rise. *J. Phys. Oceanogr.* **24**, 1512–1531.

Clarke, R. A., Hill, H. W., Reiniger, R. R. and Warren, B. 1980. Current system south and east of the Grand Banks of Newfoundland. *J. Phys. Oceanogr.* **10**, 25–65.

Ezer, T. and Mellor, G. L. 1992. A numerical study of the variability and the separation of the Gulf Stream induced by surface atmospheric forcing and lateral boundary flows. *J. Phys. Oceanogr.* **22**, 660–682.

Ezer, T. 1994. On the interaction between the Gulf Stream and the New England Seamount Chain. *J. Phys. Oceanogr.* **24**, 191–204.

Fofonoff, N. and Hendry, R. 1985. Current variability near the southeast Newfoundland Ridge. *J. Phys. Oceanogr.* **15**, 963–984.

Klein, B. and Siedler, G. 1989. On the origin of the Azores Current. *J. Geophys. Res.* **94**, 6159–6168.

Krauss, W., Case, R. H. and Hinrichsen, H.-H. 1990. The branching of the Gulf Stream Southeast of the Grand Banks. *J. Geophys. Res.* **95**, 13089–13103.

Long, R. R. 1955. Some aspects of the flow of stratified fluids III, continuous density gradients. *Tellus* **7**, 342–357.

Mann, C. 1967. The termination of the Gulf Stream and the beginning of the North Atlantic Current. *Deep Sea Res.* **14**, 337–359.

Mellor, G. 1993. *A three-dimensional, primitive equation, numerical ocean model.* Atmos. and Oceanic Sciences Program, Princeton Univ. technical report, 35 pp.

Oey, L.-Y., Ezer, T., Mellor, G. L. and Chen, P. 1992. A model study of "bump" induced western boundary current variabilities. *J. Mar. Sys.* **3**, 321–342.

Richardson, P. L. 1993. A census of eddies observed in North Atlantic SOFAR float data. *Prog. Oceanogr.* **31**, 1–50.

Shi, C. and Chao, S.-Y. 1994. Eastward jets over diverging isobaths with applications to the Gulf Stream past the Grand Banks. *J. Geophys. Res.* **99**, 22689–22706.

Sy, A. 1988. Investigation of large-scale circulation patterns in the central North Atlantic: The North Atlantic Current, the Azores Current, and the Mediterranean Water plume in the area of the Mid-Atlantic Ridge. *Deep-Sea Res.* **35**, 383–413.

Warren, B. 1969. Divergence of isobaths as a cause of current branching. *Deep Sea Res.* **16**, 339–355.

Yih, C.-S. 1980. *Stratified flows.* Academic press, 418 pp.